IEEE Access
Multidisciplinary | Rapid Review | Open Access Journal

SPECIAL SECTION ON DATA-ENABLED INTELLIGENCE FOR DIGITAL HEALTH

Received February 28, 2019, accepted March 18, 2019, date of publication March 28, 2019, date of current version April 12, 2019.

Digital Object Identifier 10.1109/ACCESS.2019.2907249

Centralized Wavelet Multiresolution for Exact Translation Invariant Processing of ECG Signals

BINQIANG CHEN, YANG LI, AND NIANYIN ZENG, (Member, IEEE)
School of Aerospace Engineering, Xiamen University, Xiamen 361005, China
Shenzhen Research Institute of Xiamen University, Shenzhen 518000, China

Corresponding author: Nianyin Zeng (zny@xmu.edu.cn)

This work was supported in part by the National Natural Science Foundation of China under Grant 51605403, in part by the Natural Science Foundation of Guangdong Province, China, under Grant 2015A030310010, and in part by the Natural Science Foundation of Fujian Province, China, under Grant 2016J01012.

ABSTRACT Dyadic wavelet transform is useful in analyzing electrocardiogram (ECG) signals due to its fast computation and its multiresolution ability. In order to improve the feature extraction performance of dyadic wavelet transform, a new construction example of centralized multiresolution (CMR) is proposed. The proposed CMR example consists of two elements, namely, a dyadic part and a non-dyadic part. The dyadic part, based on the maximal overlap second generation wavelet packet transform (SGWPT), generates dyadic wavelet packets. The non-dyadic part engenders ensemble wavelet packets by postprocessing on the dyadic part. The produced wavelet packets and ensemble wavelet packets are combined to realize continued spectral refinement around fixed central analysis frequencies. Numerical simulation and a case study of ECG signal decomposition are utilized to validate the enhancements of the proposed CMR example. The processing results of the CMR example are compared with those of the dual tree complex wavelet transform and the conventional SGWPT. It is validated this CMR example achieves better feature extraction performances due to the presence of the exact translation invariance property.

INDEX TERMS Wavelet transform, electrocardiogram, centralized multiresolution analysis, translation invariance.

I. INTRODUCTION

Heart disease and heart stroke is a major threat to human life [1]. The electrocardiogram (ECG) is the acquisition of cardiac activities using noninvasive techniques. It provides valuable information about bio-electric potentials corresponds with the contractions and relaxations of the heart muscle [2]. The ECG forms the core amongst the lifesaving diagnostic tools in the heartcare segment [3]. Therefore, long-term monitoring of this physical process is highly recommended for patients who are suffering from the cardiovascular disease.

Typically, an ECG signal is composed of characteristic features of P, QRS complex and T points (Figure 1) [4]. In the literature, numerous methodologies have been developed to investigate these characteristic features such that cardiac diseases can be revealed [5]. However, the ECG signal is by nature a multi-component and non-stationary time series. On the other hand, the measured ECG signals are usually corrupted by interferences such as baseline wanders, power line interferences and physiological artefacts. To eliminate negative effects induced by these noises, ECG feature detection methodologies enhanced by preprocessing stages and postprocessing stages are necessary. A comprehensive review of ECG detection methodologies is presented in Refs. [5]–[8]. The existing ECG detection methodologies aim to improve the detection accuracy via sophisticated signal processing

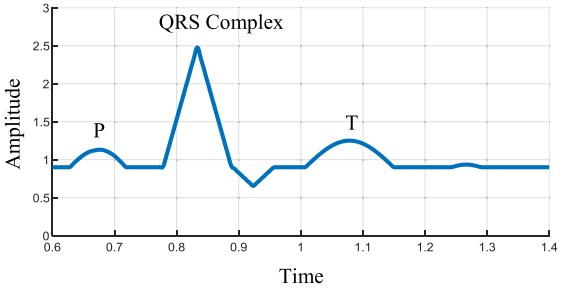

FIGURE 1. The basic pattern of a typical ECG signal.

The associate editor coordinating the review of this manuscript and approving it for publication was Yonghong Peng.

techniques. Some of the popular detection methodologies can be numerated as spectrum analysis methods (Fourier transform and short-time Fourier transform) [9], [10], mathematical morphology [11], wavelet transform (WT) [12], empirical mode decomposition (EMD) [13], blind source separation [14], and sparsity based strategies [15].

WT is derived from the conventional Fourier transform by introducing multiresolution analysis [16]. It has proven to be an effective and efficient tool in biomedical fields [17]–[19]. In the past decades, a number of variations of WT have been developed and applied in biomedical signal analysis applications [16], [17]. In many researches, WT is usually adopted in preprocessing stages of ECG feature analysis. Hamaneh attempted to remove electrocardiographic artifacts using a technique based on the combination of independent component analysis and continuous wavelet transform (CWT) [19]. However, a major disadvantage of CWT is its high computational burden. Comparatively, discrete wavelet transform is more efficient because it decomposes an input signal into a few frequency subbands using a single scaling function and a single wavelet function [20], [21]. Benzid utilized discrete wavelet transform in the ECG signal decomposition [22]. Poungponsri and Yu proposed an adaptive filtering approach based on the discrete wavelet transform and the artificial neural network for ECG signal noise reduction [23]. Zou *et al.* designed a low power biomedical device to implement discrete wavelet transform for QRS complex detection [24]. Yu and Chen studied the electrocardiogram beat classification problem through high order statistics on six wavelet components extracted from ECG signals [25]. Hassan and Haque utilized a data-adaptive signal decomposition scheme (tunable-Q wavelet transform) to decompose segments of ECG signals [26]. Thomas *et al.* proposed a dual tree complex wavelet transform (DTCWT) based feature extraction technique for automatic classification of cardiac arrhythmias [12]. Kumar *et al.* employed flexible analytic wavelet transform to extract multiscale features of ECG signals in diagnosis of the coronary artery disease [27].

Among the multiple variations of discrete wavelet transform, there are still some inevitable shortcomings [28], [29]. For both of the dyadic wavelet decomposition and the associated discrete wavelet packet decomposition, no matter which wavelet basis is chosen, their frequency-scale paving patterns are identical and fixed [30], [31]. Their performances are relatively poor in extracting transition band features [21]. For overcomplete discrete wavelet transform characterized by a few free parameters, nonconventional upsampling operators and nonconventional downsampling operators are introduced [17], [21]. However, more than one wavelet decomposition is usually required to make a comprehensive investigation of the hidden features [28]. In 2018, an improved theory of centralized multiresolution (CMR) analysis was proposed by Chen and Zeng [20], [21]. The CMR is a novel type of wavelet decomposition constructed based on dyadic wavelet analysis. A concrete construction example was given by postprocessing of DTCWT. CMR can engender multiresolution around some specific spectral bins [32]. Although this construction example inherits many merits of DTCWT, it is still not of exact translation invariance, which plays an important role in nonstationary feature analysis.

In order to address this problem, we attempt to construct another concrete example of CMR, which is equipped with property of exact translation invariance, based on the second generation wavelet theory [33]–[36]. In the new construction example of CMR, the input signal is firstly decomposed by maximal overlap second generation wavelet packet transform (MOSGWPT) into dyadic wavelet packet subspaces. To enhance the analyzing performance for transition band features, an ensemble wavelet packet generating strategy is introduced to produce ensemble wavelet packets (EWPs) whose central analysis frequencies (CAFs) are located at edges of the dyadic frequency-scale pattern. Properties of the new construction example (frequency-scale pattern, time-frequency atom, and exact shift invariance) are studied to show its superiorities. The frequency-scale pattern of the new example is investigated to reveal the valuable merit of centralized multiresolution. The property of exact shift invariance is verified by applying decompositions on shifted discrete Dirac sequences. Moreover, it is also found that time-frequency atoms of both dyadic wavelet packets and EWPs are symmetric, therefore reducing distortions in the multiscale decomposition [37], [38].

The new construction example was used to decompose ECG signals from MIT-BIH arrhythmia database. As comparison, the DTCWT and the conventional second generation wavelet packet transform are also employed to process the same ECG signals. It is validated that properties of centralized multiresolution and the property of exact translation invariance are both beneficial in feature extraction of ECG signals.

II. FUNDAMENTALS OF CONVENTIONAL DISCRETE WAVELET THEORY

A. DYADIC WAVELET TRANSFORM

In wavelet analysis, dyadic wavelet transform (DWT) is widely used due to its fast computation. Wavelet coefficients are obtained using inner product transforms between input signals and time-frequency atoms.

$$WT_{a,b}(x) = \frac{1}{\sqrt{a}} \int_{-\infty}^{+\infty} x(t)\psi\left(\frac{t-b}{a}\right) dt, \tag{1}$$

where $x(t)$ is the input signal and $\psi(t)$ is the time-frequency atom.

The time-frequency atoms of dyadic wavelet transform are generated via dilations and translations from a scaling function $\phi(t)$ and a wavelet function $\psi(t)$. $\phi_{j,k}(t)$ and $\psi_{j,k}(t)$ can be expressed as

$$\begin{aligned} \phi_{j,k}(t) &= \phi(2^j t - k) \\ \psi_{j,k}(t) &= \psi(2^j t - k), \end{aligned} \tag{2}$$

where the integer j denotes the decomposition stage; the integer k denotes the translation in the time domain; and Z denotes the set of complex number. Let the corresponding discrete finite impulse response functions of $\phi(t)$ and $\psi(t)$ be represented as $h(n)$ and $g(n)$, two-scale relationships exist for these time-frequency atoms.

$$\phi(t) = \sum_{n\in\mathbb{Z}} h(n)\phi(2t-n), \tag{3}$$

$$\psi(t) = \sum_{nn\in\mathbb{Z}} g(n)\psi(2t-n). \tag{4}$$

The implementation filterbank of the dyadic wavelet transform is shown in Figure 2, where $H(w)$ and $G(w)$ represent Fourier counterparts of finite support filters $h(n)$ and $g(n)$. As can be observed, the DWT decomposes the low frequency bands iteratively. It should be noticed that downsampling operations in the decomposition process and upsampling operations in the synthesis process will cause a side effect of translation variance in signal analysis.

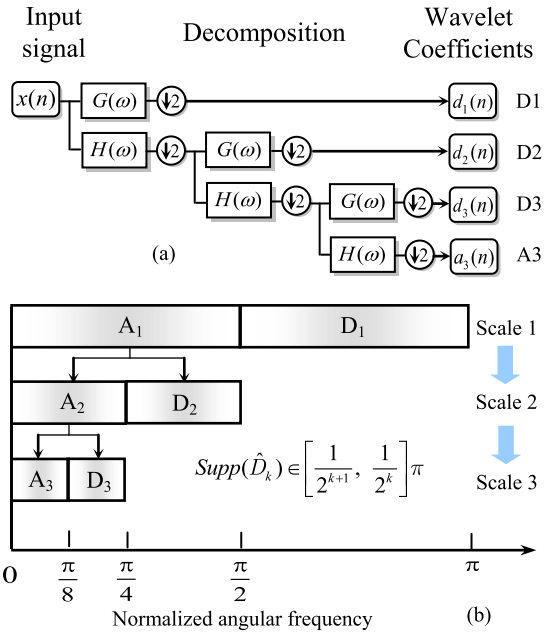

FIGURE 2. Filterbank structure of dyadic wavelet transform: (a) the decomposition process; and (b) the frequency-scale paving.

B. DYADIC WAVELET PACKET DECOMPOSITION

The wavelet packet decomposition (WPD) is developed as an extension of the dyadic wavelet transform. In WPD, the higher frequency subbands are further decomposed via the iterated tree-structured implementation filterbanks displayed in Figure 3. Let $x(n)$ be a discrete time series of length L and f_s be the sampling frequency. The frequency-scale pattern of multi-stage WPD is shown in Figure 4. It can be inferred that each wavelet packet possesses a unique CAF, which is marked by the purple dashed line. As such, either DWT or WPD is not perfect in extracting transient band features whose spectral counterparts lie in transition areas of dyadic grids (Figure 5).

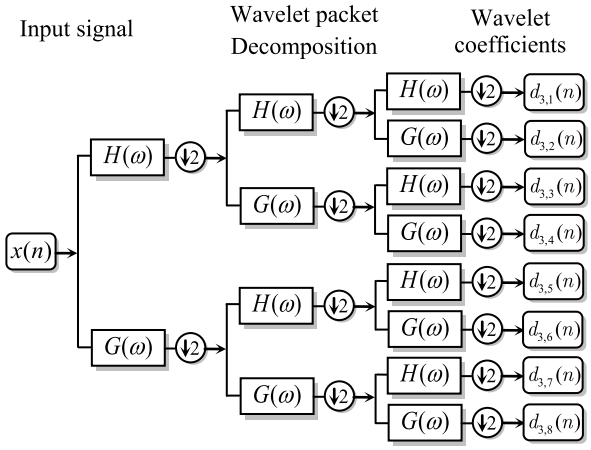

FIGURE 3. The tree-structured filterbank structure for WPD.

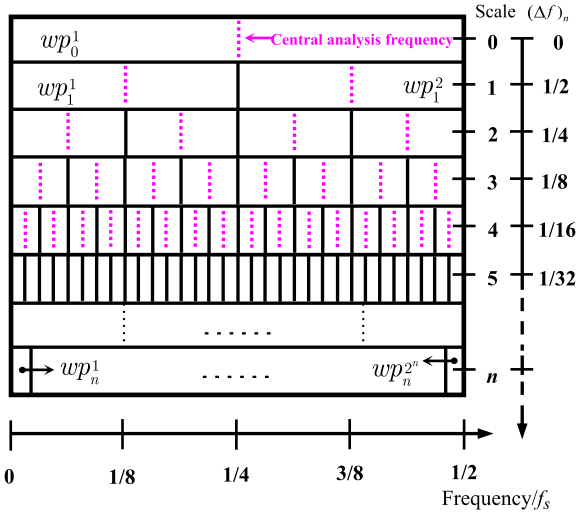

FIGURE 4. The frequency-scale pattern of dyadic wavelet packet decomposition.

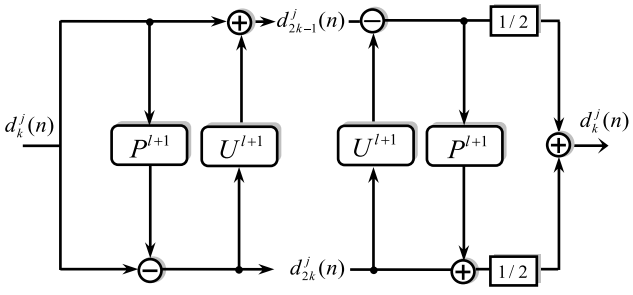

FIGURE 5. Implementation structure of maximal overlap lifting scheme.

III. NOVEL CMR CONSTRUCTION EXAMPLE BASED ON SECOND GENERATION WAVELET TRANSFORM

A. MAXIMAL OVERLAP LIFTING SCHEME FOR WAVELET PACKET DECOMPOSITION

The second generation wavelet is essentially a biorthogonal wavelet transform that can be implemented not only by

the tree-structured filterbanks but also by a special lifting scheme. To ensure translation-invariance, a maximal overlap lifting scheme (MOLS) is utilized. Let the prediction operator and the update operator be represented by P and U respectively, the MOLS (Figure 5) can be implemented via the following framework. That is to say, the numbers of samples in each wavelet packet coefficient series are identical to that of the input signal.

In Figure 5, The coefficient of P^l and U^l are obtained by padding the original P, of length N_P and U by zeros, of length N_U.

$$P^l = [p_1, \underbrace{0\ldots0}_{2^l-1}, p_2, \ldots, p_{N_P-1}, \underbrace{0\ldots0}_{2^l-1}, p_{N_P}] \quad (5)$$

$$U^l = [u_1, \underbrace{0\ldots0}_{2^l-1}, p_2, \ldots, p_{N_U-1}, \underbrace{0\ldots0}_{2^l-1}, p_{N_U}] \quad (6)$$

For an input series $x(n)$, a j-stage MOSGWPT can generate 2^j wavelet packet coefficient series, namely $\{d_{j,1}, d_{j,2}, \ldots d_{j,2^j}\}$. In the forward transform, the algorithm can be divided into two sub-steps.

Step 1) Predict step

$$\tilde{d}_{j,2k-1}(n) = d_{j,k}(n) - \sum_{\ell=1}^{(N_P-1)2^j+1} p^j(\ell) d_{j,k}(n+\ell) \quad (7)$$

Step 2) Update step

$$d_{j,2k-1}(n) = d_k^j(n) + \sum_{\ell=1}^{(N_P-1)2^j+1} p^j(\ell) \tilde{d}_{j,2k}(n+\ell) \quad (8)$$

The algorithm of the inverse transform can be divided into three sub-steps.

Step 1) Inverse update step

$$\tilde{d}_{j,2k-1}(n) = d_{j,2k-1}(n) - \sum_{\ell=1}^{(N_U-1)2^j+1} u^j(\ell) d_{j,2k}(n+\ell) \quad (9)$$

Step 2) Inverse predict step

$$\tilde{d}_{j,2k}(n) = d_{j,2k}(n) + \sum_{\ell=1}^{(N_P-1)2^j+1} p^j(\ell) d_{j,2k-1}(n+\ell) \quad (10)$$

Step 3) Merge step

$$\hat{d}_{j,k}(n) = \frac{1}{2}\left[\tilde{d}_{2k-1}^{(j)}(n) + \tilde{d}_{2k}^{(j)}(n)\right] \quad (11)$$

The flow chart of this algorithm is shown in Figure 6.

B. CONSTRUCTION OF NON-DYADIC ENSEMBLE WAVELET PACKETS

A novel strategy is introduced to construct non-dyadic wavelet packet subspaces. The algorithm can be divided into the following steps.

Step 1) MOSGWPT of the input signal $\{x(n)\}$, represented as

$$x(n) \mapsto wpc_j := \{d_{j,k}(n) | k = 1, 2, \ldots, 2^j\}. \quad (12)$$

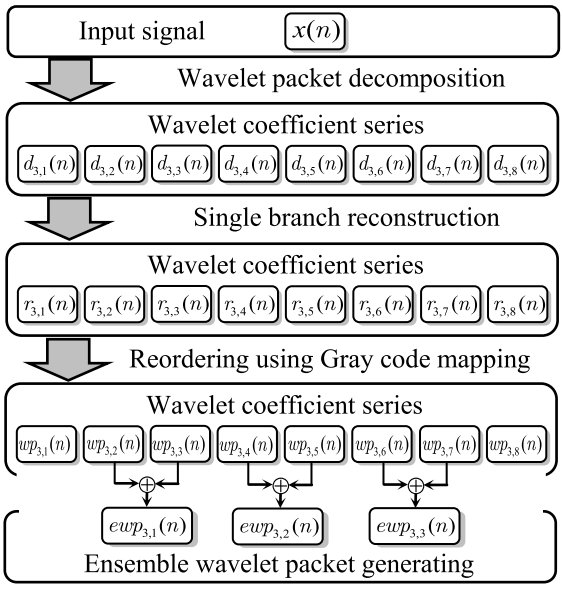

FIGURE 6. Implementation structure of maximal overlap lifting scheme.

Step 2) Single branch reconstruction of wpc_j.

$$wpc_j \mapsto wpr_j := \{r_{j,1}(n), \quad r_{j,2}(n), \ldots, r_{j,2^j}(n)\}. \quad (13)$$

Step 3) Reorder the elements in wpr^j using Gray code mapping such that the elements are placed in ascending order of CAF value.

$$wpc_j \mapsto wp_j := \{wp_{j,1}(n), \quad wp_{j,2}(n), \ldots, wp_{j,2^j}(n)\}. \quad (14)$$

Step 4) Generate ensemble wavelet packets by superposition of adjacent wavelet packets

$$ewp_{j,k}(n) = wp_{j,2k}(n) + wp_{j,2k}(n). \quad (15)$$

The flow chart of the proposed algorithm is shown in Figure 6. For an integer k, the procedure of the mentioned Gray code mapping is shown as below. In binary coding, the integer i is expressed as

$$i = \sum_{k=0}^{j-1} 2^k n_k, \quad (16)$$

where the variable is ranged in $\{0, 1\}$. Then another integer $\tilde{i}$ is defined as

$$\tilde{i} = \sum_{k=0}^{j-1} 2^k \tilde{n}_k. \quad (17)$$

The mapping between $\{n_i\}$ and $\{\tilde{n}_i\}$ is described as

$$\tilde{n}_k = \begin{cases} n_k & for\ k = j-1 \\ \mathrm{mod}(n_k + n_{k+1}, 2) & for\ k = 0, 1, \ldots, j-2, \end{cases} \quad (18)$$

where $\mathrm{mod}(\cdot,\cdot)$ stands for the modular operation in mathematics.

TABLE 1. Comparisons of CAFs and pass band frequency.

Decomposition Method	Central analysis frequency (CAF)	Pass band width (PBW)
Dyadic wavelet packet $wp_{j,k}$	$\frac{k+0.5}{2^j} f_s$	$\frac{1}{2^j} f_s$
Centralized multiresolution $ewp_{j,k}$	$\frac{k}{2^{j-1}} f_s$	$\frac{1}{2^{j-1}} f_s$

IV. PROPERTIES OF THE CMR CONSTRUCTION EXAMPLE

In this section we investigate properties and merits of the novel construction example of CMR. The properties include a centralized frequency-scale pattern and the exact translation invariance.

A. NON-DYADIC FREQUENCY-SCALE PAVING

The frequency-scale pattern of the new construction example is shown in Figure 7. With the increasing of decomposition stages, the frequency resolutions of EWPs are continuously refined by a factor of 1/2, which is similar with DWT and WPD. However, it is found that there are groups of EWPs sharing identical CAFs. In other words, a phenomenon of multiresolution around some specific CAFsis observed. This phenomenon is referred to as the novel concept of centralized multiresolution. In Table 1, we list the CAFs and pass band widths of subspaces belonging to SGWPT and those of the CMR example. The CAFs of the CMR example are located at edges of pass band of dyadic wavelet packets, which is beneficial in extracting transition band features mentioned above.

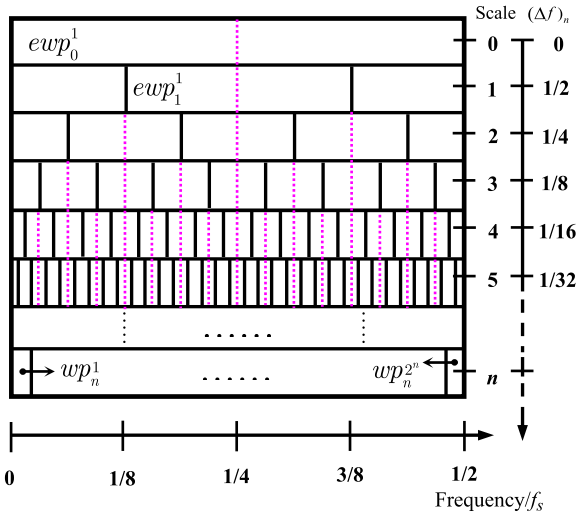

FIGURE 7. Frequency-scale pattern of the new construction example.

B. EXACT TRANSLATION INVARIANCE

The property of exact translation invariance is beneficial in analyzing periodical and nonstationary features. To demonstrate the exact translation invariance of the construction example, the discrete Dirac function, whose definition is given in Equation (19), is used.

$$\delta(n) = \begin{cases} 1 & n = 0 \\ 0 & others, \end{cases} \tag{19}$$

where $n, n_0 \in Z$. By performing multiscale decompositions on shifted discrete Dirac sequences $\delta(n - n_0)$, we have the decomposition results in Figure 8.

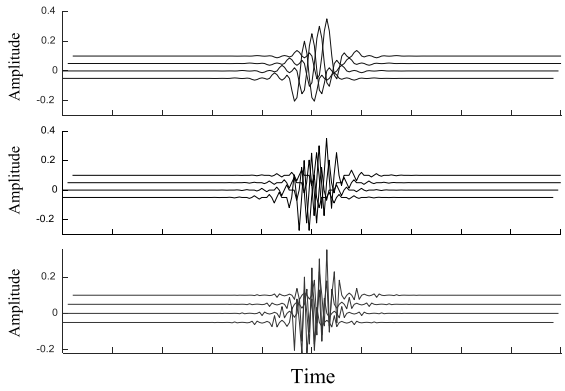

FIGURE 8. Exact translation invariance of ensemble wavelet packets.

V. INVESTIGATIONS OF CMR CONSTRUCTION EXAMPLE IN MULTISCALE DECOMPOSITION

In this section, we investigate the superiority of the new CMR example in multi-component signal analysis. A simulation signal comprising multiple simple harmonic waves is simulated as below.

$$x(t) = \cos(2\pi 90t) + \cos(2\pi 340t) + \cos(2\pi 650t) + \cos(2\pi 910t). \tag{20}$$

The sampling frequency and the sampling length of the signal are set as 2000 and 2000 respectively. The time domain waveform and the associated Fourier spectrum are plot in Figure 9. The spectral resolution of the signal is calculated at 1Hz.

The decomposition results of the simulated multi-component signal using the CMR construction example is shown in Figure 10. The four extracted components are

$$\{c_{cmr1}(n), \quad c_{cmr2}(n), \ c_{cmr3}(n), \ c_{cmr4}(n)\}. \tag{21}$$

It can be observed from the figure that the four simple harmonic components coupled in the time domain are successfully separated with relatively small waveform distortions. As comparisons, the simulated signal is also decomposed by the dual tree complex wavelet analysis. The four extracted components are

$$\{c_{dt1}(n), \quad c_{dt2}(n), \ c_{dt3}(n), \ c_{dt4}(n)\}. \tag{22}$$

In Figure 11, we plot the waveforms of the four extracted components. The results by the DTCWT and those of the CMR construction example are very similar. The reason for

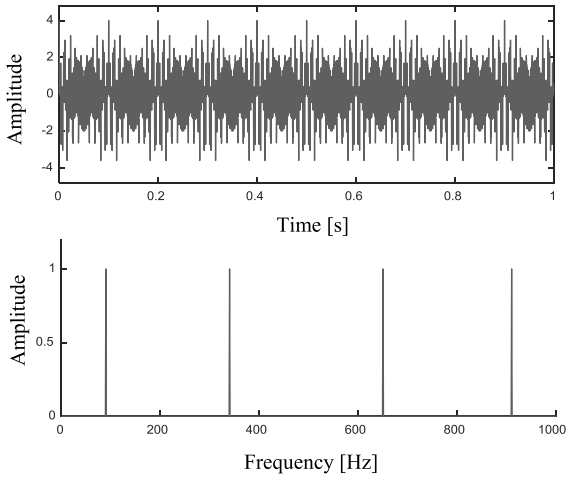

FIGURE 9. The simulated multi-component signal.

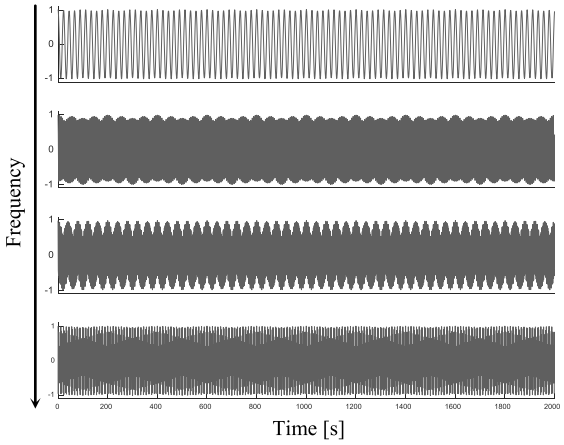

FIGURE 10. Decomposition results by the new CMR construction example.

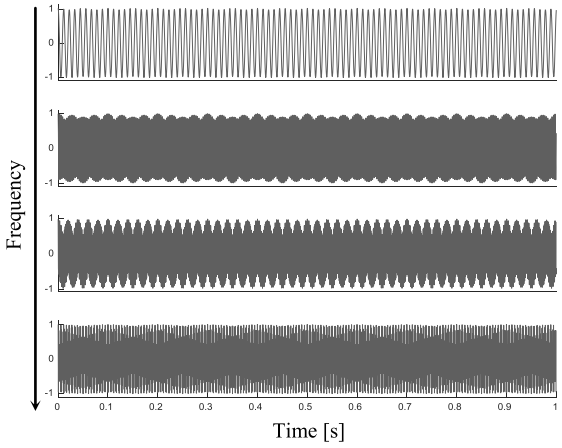

FIGURE 11. Decomposition results by the new CMR construction example.

their similarities lies in the fact that the DTCWT is nearly translation invariant and nearly analytic.

The conventional second generation wavelet packet transform is also employed to process the simulated signal. The four extracted components are

$$\{c_{sg1}(n), \quad c_{sg2}(n), \ c_{sg3}(n), \ c_{sg4}(n)\}. \tag{23}$$

Their waveforms are shown in Figure 12. Owing the lack of translation invariance, considerable waveform distortions occur on the single branch reconstruction signals. Especially for slow-varying wavelet packets, the phenomenon of artificial modulation is detected, which severely corrupt the extracted components.

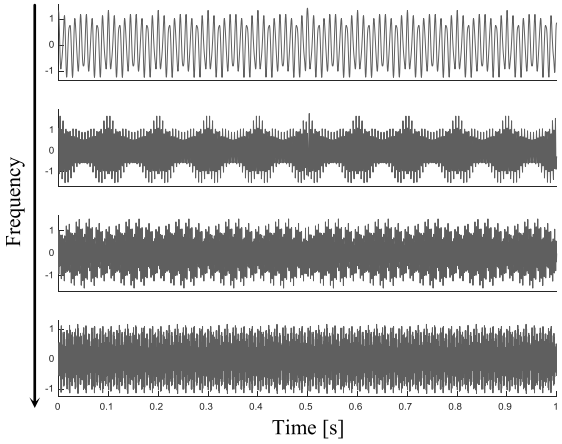

FIGURE 12. Decomposition results by conventional second generation wavelet packet transform.

To make further comparisons, the indicator of correlation coefficient (CC) is utilized. The mathematical definition of the correlation coefficient between the input series of $x(n)$ and $y(n)$ is given as below.

$$Corr[x(n), y(n)] = \frac{E[(x - \mu_x)(y - \mu_y)]}{\sigma_x \sigma_y}, \tag{24}$$

where μ_x and μ_y denote the mean value of the input series; σ_x and σ_y denote the standard variation of the input series; and the operator $E[\cdot]$ means the mathematical expectation in statistical analysis. Higher values of CC indicate higher similarities between the two input series. For each decomposition method, we calculate the CCs between the original components and the extracted components. The results are listed in Table 2.

TABLE 2. Correlation coefficients generated by the three decomposition methods.

	Extracted component 1	Extracted component 2	Extracted component 3	Extracted component 4
CMR	0.9998	0.9998	0.9998	0.9999
DTCWT	0.9997	0.9989	0.9993	0.9998
SGWPT	0.9701	0.9138	0.9318	0.9861

Another visual representation of the data in Table 2 is shown in the bar plot of Figure 13.

For each component, the results by the CMR construction example exhibit the greatest value of correlation coefficient,

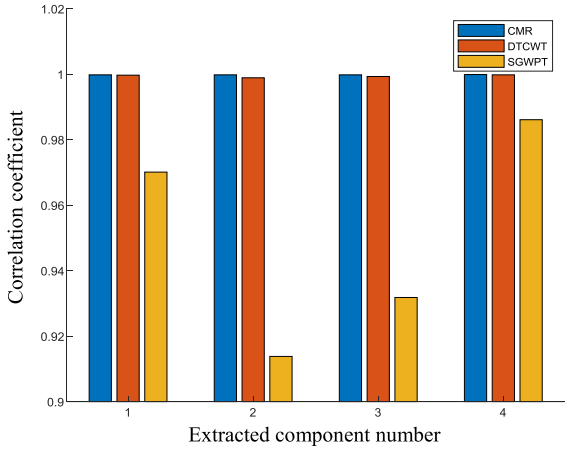

FIGURE 13. Correlation coefficients between the original components and the extracted components.

indicating the best feature multi-component separation performances. While the CCs calculated from results by the conventional SGWPT are smallest in value. It is sufficient to conclude that better translation invariance ensures better feature extraction ability.

VI. APPLICATION IN ECG SIGNAL ANALYSIS

The analyzed ECG data in this section is shared by Massachusetts Institute of Technology and Beth Israel hospital (MIT-BIH) arrhythmia database. The ECG signal was digitized at 360 samples per second. A record of signal of 10 seconds is adopted in this case study. The time domain waveform and its Fourier spectrum are shown in Figure 14.

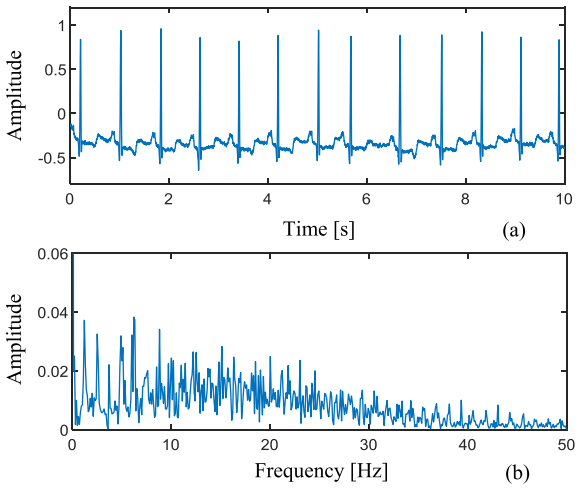

FIGURE 14. Information of the analyzed ECG signal: (a) the time domain waveform; and (b) the Fourier spectrum.

In the time domain, noises are detected between the impulses. It can be inferred from the Fourier spectrum that the energy of the contents is spread in a wide frequency range. Considering the nonstationary nature, the amplitude distribution of the ECG signal using the continuous wavelet

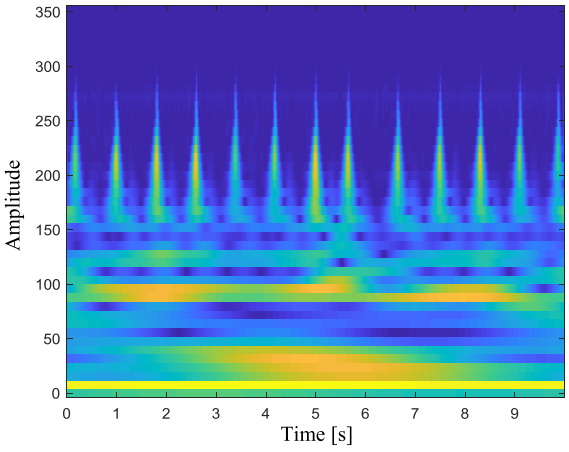

FIGURE 15. Amplitude distribution of the analyzed ECG signal using continuous wavelet transform.

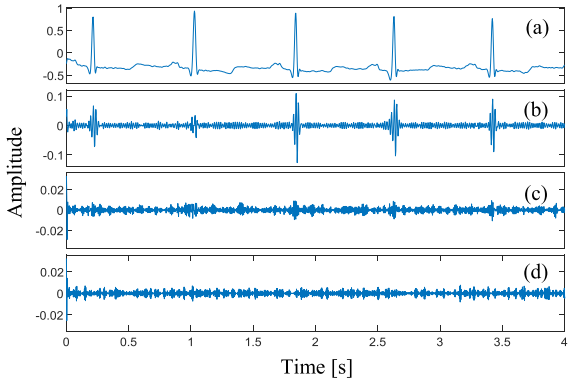

FIGURE 16. Decomposition results of the ECG signal by the CMR example: (a) $c_{cmr1}(n)$; (b) $c_{cmr2}(n)$; (c) $c_{cmr3}(n)$; (d) $c_{cmr4}(n)$.

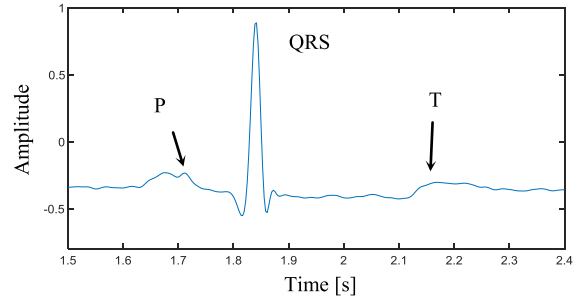

FIGURE 17. Zoom-in plot of the denoised ECG signal.

transform is plot in Figure 15. In this figure, transient features of broadband spectrum are also revealed.

The proposed CMR example was applied to decompose the signal. The related single branch reconstruction signals are shown in Figure 16. The noises are decomposed into wavelet subspaces of higher frequency range. In the zoom-in plot (Figure 17), the characteristic features of P, QRS complex and T points are successfully extracted, while the noises in the original measurement are effectively suppressed.

As comparison, the ECG signal is also processed by the DTCTW and the conventional SGWPT. In the results generated by the DTCWT (Figure 18), although the noises in the

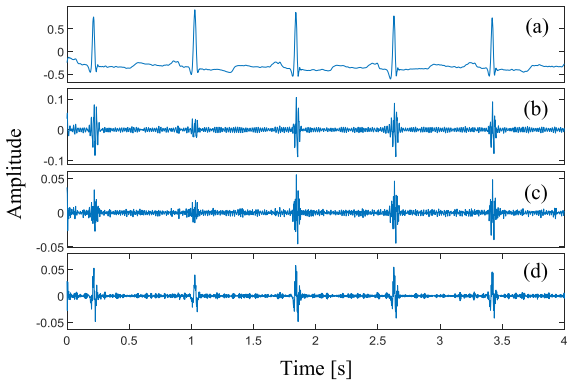

FIGURE 18. Decomposition results of the ECG signal by DTCWT: (a) $c_{dt1}(n)$; (b) $c_{dt2}(n)$; (c) $c_{dt3}(n)$; (d) $c_{dt4}(n)$.

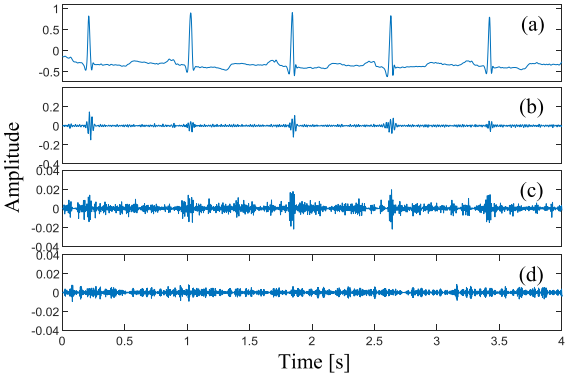

FIGURE 19. Decomposition results of the ECG signal by the conventional SGWPT: (a) $c_{sg1}(n)$; (b) $c_{sg2}(n)$; (c) $c_{sg3}(n)$; (d) $c_{sg4}(n)$.

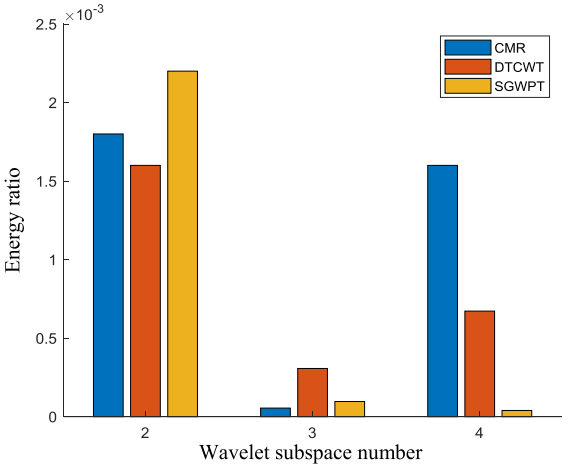

FIGURE 20. Energy ratios between the higher frequency subspaces and the lowest frequency subspace.

lower frequency range have been suppressed, the mode of the impulses has cracked into many subspaces. Comparing the results of Figure 17 with those in Figure 18, it is confirmed that the property of exact translation invariance is crucial in multi-component separation applications.

The processing results of the ECG signal by the SGWPT are given in Figurer 19. The mode crack phenomenon is also found in subspaces in higher frequency range.

To make further and quantitative comparisons on the performances of the above three method, the energy ratios between higher frequency subspaces and the first subspace are calculated. The results are shown in Figure 20. Because all of the energy ratios are low in value, all of these three methods can suppress the measurement noises. Checking the results in Figure (16-20), it is confirmed that the property of exact translation invariance can better preserve the original waveform as well as suppressing the mode crack phenomenon.

VII. CONCLUSION

In this paper, a novel construction example, capable of realizing centralized multiresolution, is proposed. The frequency-scale pattern of the proposed CMR example is expanded by a dyadic part and a non-dyadic part, where the latter possesses an improved performance in extracting transition band features in the dyadic frequency-scale pattern. The proposed example is based on the maximal overlap second generation wavelet packet analysis, and therefore it inherits the attractive merit of exact translation invariance. A multi-component signal is simulated to verify the superiority of this valuable merit. It is found it can better preserve the feature waveforms after single branch reconstruction in wavelet decompositions. The proposed CMR example, the DTCWT, the conventional SGWPT are used to process an ECG signal from MIT-BIH arrhythmia database. The processing results show that the proposed CMR example is equipped with better performance in suppressing noises and extracting nonstationary features.

REFERENCES

[1] S. Sahoo, B. Kanungo, S. Behera, and S. Sabut, "Multiresolution wavelet transform based feature extraction and ECG classification to detect cardiac abnormalities," *Measurement*, vol. 108, pp. 55–66, Oct. 2017.

[2] A. Awal, S. S. Mostafa, M. Ahmad, and M. A. Rashid, "An adaptive level dependent wavelet thresholding for ECG denoising," *Biocybernetics Biomed. Eng.*, vol. 34, no. 4, pp. 238–249, 2014.

[3] M. Merah, T. A. Abdelmalik, and B. H. Larbi, "R-peaks detection based on stationary wavelet transform," *Comput. Methods Programs Biomed.*, vol. 121, no. 3, pp. 149–160, Oct. 2015.

[4] S. Yazdani and J. M. Vesin, "Extraction of QRS fiducial points from the ECG using adaptive mathematical morphology," *Digit. Signal Process.*, vol. 56, pp. 100–109, Sep. 2016.

[5] B.-U. Kohler, C. Hennig, and R. Orgleister, "The principles of software QRS detection," *IEEE Eng. Med. Biol. Mag.*, vol. 21, no. 1, pp. 42–57, Jan./Feb. 2002.

[6] I. Beraza and I. Romero, "Comparative study of algorithms for ECG segmentation," *Biomed. Signal Process. Contr.*, vol. 34, pp. 166–173, Apr. 2017.

[7] M. Elgendi, B. Eskofier, S. Dokos, and D. Abbott, "Revisiting QRS detection methodologies for portable, wearable, battery-operated, and wireless ECG systems," *PLoS One*, vol. 9, no. 1, 2014, Art. no. e84018.

[8] S. Jain, M. K. Ahirwal, A. Kumar, V. Bajaj, and G. K. Singh, "QRS detection using adaptive filters: A comparative study," *ISA Trans.*, vol. 66, pp. 362–75, Jun. 2017.

[9] M. G. Tsipouras and D. I. Fotiadis, "Automatic arrhythmia detection based on time and time–frequency analysis of heart rate variability," *Comput. Methods Progr. Biomed.*, vol. 74, no. 2, pp. 95–108, 2004.

[10] L. G. Gamero, J. Vila, and F. Palacios, "Wavelet transform analysis of heart rate variability during myocardial ischaemia," *Med. Biol. Eng. Comput.*, vol. 40, pp. 72–78, Jan. 2002.

[11] T. Y. Ji and Q. H. Wu, "Broadband noise suppression and feature identification of ECG waveforms using mathematical morphology and embedding theorem," *Comput. Methods Programs Biomed.*, vol. 112, no. 3, pp. 466–480, 2013.
[12] M. Thomas, M. K. Das, and S. Ari, "Automatic ECG arrhythmia classification using dual tree complex wavelet based features," *AEU-Int. J. Electron. Commun.*, vol. 69, no. 4, pp. 715–721, 2015.
[13] M. Suchetha, N. Kumaravel, M. Jagannath, and S. K. Jaganathan, "A comparative analysis of EMD based filtering methods for 50 Hz noise cancellation in ECG signal," *Inform. Med. Unlocked*, vol. 8, pp. 54–59, 2017.
[14] S. Ziani, A. Jbari, L. Bellarbi, and Y. Farhaoui, "Blind maternal-fetal ECG separation based on the time-scale image TSI and SVD—ICA methods," *Procedia Comput. Sci.*, vol. 134, pp. 322–327, 2018.
[15] G. Da Poian, R. Bernardini, and R. Rinaldo, "Separation and analysis of fetal-ECG signals from compressed sensed abdominal ECG recordings," *IEEE Trans. Biomed. Eng.*, vol. 63, no. 6, pp. 1269–1279, Jun. 2016.
[16] B. Chen, Z. Zhang, Y. Zi, Z. He, and C. Sun, "Detecting of transient vibration signatures using an improved fast spatial–spectral ensemble kurtosis kurtogram and its applications to mechanical signature analysis of short duration data from rotating machinery," *Mech. Syst. Signal Process.*, vol. 40, no. 1, pp. 1–37, 2013.
[17] K. Tanaka and A. R. Hargens, "Wavelet packet transform for R-R interval variability," *Med. Eng. Phys.*, vol. 26, no. 4, pp. 313–319, 2004.
[18] S. Bilgin, O. H. Çolak, E. Koklukaya, and N. Arı, "Efficient solution for frequency band decomposition problem using wavelet packet in HRV," *Digit. Signal Process.*, vol. 18, pp. 892–899, Nov. 2008.
[19] M. B. Hamaneh, N. Chitravas, K. Kaiboriboon, S. D. Lhatoo, and K. A. Loparo, "Automated removal of EKG artifact from EEG data using independent component analysis and continuous wavelet transformation," *IEEE Trans. Biomed. Eng.*, vol. 61, no. 6, pp. 1634–1641, Jun. 2014.
[20] X. Cao, N. Zeng, B. Chen, and W. He, "Sparsity enhanced topological fractal decomposition for smart machinery fault diagnosis," *IEEE Access*, vol. 6, pp. 51886–51897, 2018.
[21] B. Chen, Z. Zhang, C. Sun, B. Li, Y. Zi, and Z. He, "Fault feature extraction of gearbox by using overcomplete rational dilation discrete wavelet transform on signals measured from vibration sensors," *Mech. Syst. Signal Process.*, vol. 33, pp. 275–298, Nov. 2012.
[22] R. Benzid, F. Marir, A. Boussaad, M. Benyoucef, and D. Arar, "Fixed percentage of wavelet coefficients to be zeroed for ECG compression," *Electron. Lett.*, vol. 39, no. 11, pp. 830–831, May 2003.
[23] S. Poungponsri and X.-H. Yu, "An adaptive filtering approach for electrocardiogram (ECG) signal noise reduction using neural networks," *Neurocomputing*, vol. 117, pp. 206–213, Oct. 2013.
[24] Y. Zou, J. Han, X. Weng, and X. Zeng, "An ultra-low power QRS complex detection algorithm based on down-sampling wavelet transform," *IEEE Signal. Proc. Lett.*, vol. 20, no. 5, pp. 515–518, May 2013.
[25] S.-N. Yu and Y.-H. Chen, "Noise-tolerant electrocardiogram beat classification based on higher order statistics of subband components," *Artif. Intell. Med.*, vol. 46, pp. 165–178, Jun. 2009.
[26] A. R. Hassan and M. A. Haque, "An expert system for automated identification of obstructive sleep apnea from single-lead ECG using random under sampling boosting," *Neurocomputing*, vol. 235, no. 26, pp. 122–130, 2017.
[27] M. Kumar, R. B. Pachori, and U. R. Acharya, "Characterization of coronary artery disease using flexible analytic wavelet transform applied on ECG signals," *Biomed. Signal Process.*, vol. 31, pp. 301–308, Jan. 2017.
[28] W. He, Y. Zi, B. Chen, F. Wu, and Z. He, "Automatic fault feature extraction of mechanical anomaly on induction motor bearing using ensemble super-wavelet transform," *Mech. Syst. Signal Process.*, vols. 54–55, pp. 457–480, Mar. 2015.
[29] W. He, Y. Ding, Y. Zi, and I. W. Selesnick, "Repetitive transients extraction algorithm for detecting bearing faults," *Mech. Syst. Signal Process.*, vol. 84, pp. 227–244, Feb. 2017.
[30] W. He, B. Chen, N. Zeng, and Y. Zi, "Sparsity-based signal extraction using dual Q-factors for gearbox fault detection," *ISA Trans.*, vol. 79, pp. 147–160, Aug. 2018.
[31] S. K. Berkaya, A. K. Uysal, E. S. Gunal, S. Ergin, S. Gunal, and M. B. Gulmezoglu, "A survey on ECG analysis," *Biomed. Signal Process. Control*, vol. 43, pp. 216–235, May 2018.
[32] X.-C. Cao, B.-Q. Chen, B. Yao, and W.-P. He, "Combining translation-invariant wavelet frames and convolutional neural network for intelligent tool wear state identification," *Comput. Ind.*, vol. 106, pp. 71–84, Apr. 2019.
[33] W. Sweldens, "The lifting scheme: A custom-design construction of biorthogonal wavelets," *Appl. Comput. Harmon. Anal.*, vol. 3, no. 2, pp. 186–200, Apr. 1996.
[34] W. Sweldens, "The lifting scheme: A construction of second generation wavelets," *SIAM J. Math. Anal.*, vol. 29, no. 2, pp. 511–546, 1998.
[35] R. L. Claypoole, G. M. Davis, W. Sweldens, and R. G. Baraniuk, "Nonlinear wavelet transforms for image coding via lifting," *IEEE Trans. Image Process.*, vol. 12, no. 12, pp. 1449–1459, Dec. 2003.
[36] H. Jiang, Z. He, C. Duan, and P. Chen, "Gearbox fault diagnosis using adaptive redundant lifting scheme," *Mech. Syst. Signal Process.*, vol. 20, no. 8, pp. 1992–2006, 2006.
[37] S. Murugesan and D. B. H. Tay, "A new class of almost symmetric orthogonal Hilbert pair of wavelets," *Signal Process.*, vol. 95, pp. 76–87, Feb. 2014.
[38] S. Abhishek, S. Veni, and K. A. Narayanankutty, "Biorthogonal wavelet filters for compressed sensing ECG reconstruction," *Biomed. Signal Process. Control*, vol. 47, pp. 183–195, Jan. 2019.

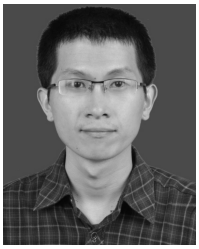

BINQIANG CHEN was born in Fuqing, Fujian, China, in 1986. He received the bachelor's degree in mechanical engineering from the School of Manufacturing Science and Technology, Sichuan University, in 2008, and the Ph.D. degree in mechanical engineering from the School of Mechanical Engineering, Xi'an Jiaotong University, in 2013. He is now an assistant professor at School of Aerospace Engineering, Xiamen University, China. His main research interests include intelligent equipment and smart manufacturing, structural health monitoring of equipment, and applied harmonic analysis.

YANG LI was born in Heze, Shandong, China, in 1994. She received the bachelor's degree in mechanical design manufacture and automation major from the School of Electromechanical and Automotive Engineering, Yantai University, in 2017. She is currently pursuing the master's degree with the School of Aerospace Engineering, Xiamen University, China. Her main research interests include intelligent equipment and smart manufacturing, and structural health monitoring of equipment.

NIANYIN ZENG was born in Longyan, Fujian, China, in 1986. He received the B.Eng. degree in electrical engineering and automation and the Ph.D. degree in electrical engineering from Fuzhou University, in 2008 and 2013, respectively.

From 2012 to 2013, he was a RA with the Department of Electrical and Electronic Engineering, The University of Hong Kong. He is currently an Associate Professor with the Department of Instrumental and Electrical Engineering, Xiamen University. He is an ISEF Fellow founded by the Korea Foundation for Advance Studies and has been a Visiting Professor with the Korea Advanced Institute of Science and Technology, since 2017. He has authored or coauthored several technical papers including five ESI Highly Cited Papers according to the most recent Clarivate Analytics ESI report and also a very active reviewer for many international journals and conferences. His current research interests include intelligent data analysis, computational intelligent, and time-series modeling and applications.

Dr. Zeng also serves as a Technical Program Committee Member for ICBEB 2014 and an Invited Session Chair of ICCSE 2017. He is currently serving as an Associate Editor for *Neurocomputing*, and also an Editorial Board Member for *Computers in Biology and Medicine*, *Biomedical Engineering Online*, the *Journal of Advances in Biomedical Engineering and Technology*, and *Smart Healthcare*.